Analysis of Load Noise Components in Small Core-Form Transformers

Keiko Yoshida, Takashi Hoshino, Seiichi Murase, Hiroshi Murakami, and Tatsuya Miyashita

***Abstract*—We propose load noise analysis components for small core-form transformers (1 MVA–20 MVA) using computational fluid-structure coupled calculations that consider the electromagnetic force, transformer structure and fluid (oil). The proposed technique has two beneficial aspects: coil modeling using shell elements of the finite element method (FEM), and acoustic noise analysis using a combination of boundary element method transmission path simulation and FEM structural simulation. The shell element model, which includes structural bending information, is less computationally intensive for simulations than solid models because it uses larger element sizes. Lighter simulations enable easier redesign for noise reduction. Additionally, division of the simulation process into individual structural vibrations, transmission paths, and radiation processes makes it easier to find a remodeling point without performing a complete simulation. We illustrate the importance of avoiding coincidence of the natural frequencies of the coils and the electromagnetic force and present a practical noise reduction study. This technique can be implemented using a light simulation that was proposed to confirm the remodeling effects. Using the proposed analysis method along with a ray tracing method, we can construct a frontloading design simulation tool to determine the transformer specifications and the substation's geographical features.**

***Index Terms*—Acoustic noise, vibration, electromagnetic force, power transformer, design for quality.**

I. Introduction

FROM the environmental impact viewpoint, the demand for low noise transformers has been increasing. It is essential to make the noise levels of these transformers conform to their surrounding environment, particularly in heavily populated areas. The small core-form transformer has a rating that is under 20 MVA. This type of transformer is often used in relatively small substations, which are generally constructed in the open air without sound-insulating walls and are sometimes located near residential areas. This rating class of transformers is used in larger numbers than transformers with ratings of more than 20 MVA. The design of power transformers with this rating should thus be regular routine work rather than custom work. Therefore, we should have conventional simulation tools for the transformer noise levels.

Transformer noise mainly originates from the following sources [1]: (a) no-load noise caused by magnetostrictive strain of the core laminations; (b) noise produced by fans or oil pumps; and (c) load noise caused by the Lorentz forces that result from interactions between the magnetic stray field of one current-carrying winding and the total electric currents within the conductors of the other winding. These forces cause vibrations in the windings that result in acoustic radiation at twice the line frequency (100 or 120 Hz).

The countermeasure for noise source (b) depends on the fan or pump devices used [2]. In addition, the frequency band of noise source (b) is a broad band, but noise sources (a) and (c) produce noise peaks at certain frequencies that tend to cause complaints within the neighborhood of the substation.

In the past, the dominant factor in causing the noise was the magnetostrictive vibration of the core [3]–[5], but following the development of 6.5% silicon steel sheets [6], [7] and step-lap cores composed of silicon steel [8], that type of noise has been greatly reduced.

In addition, the electromagnetic vibration of the coils had typically been considered to be the major factor behind vertical directional displacement. Therefore, a simple one-dimensional mass-spring analysis was used, in which the coils were modeled as mass points and the spacers used for electrical isolation between the coils were modeled as springs [9].

However, we have found that radial direction accelerations cannot be ignored because the coil vibration modes move in three dimensions, like those of disks or cylinders. Therefore, rather than use the simple mass-spring analysis, we proposed a numerical simulation using a 3D model [10]. Some other papers also proposed 3D model simulations of the transformer noise [11]–[14].

In [11], the electromagnetic vibrations of the coils were analyzed using a 3D solid finite element method (FEM) model. This solid model made it possible for the analysis to simulate the vertical and radial directional vibrations, but also requires high computing power, so it is unsuitable for use for regular routine works of small core-form transformers.

Manuscript received March 19, 2020; revised June 16, 2020, June 17, 2020, and June 20, 2020; accepted July 27, 2020. Date of publication September 28, 2020; date of current version September 23, 2021. Paper no. TPWRD-00411-2020. *(Corresponding author: Keiko Yoshida.)*

Keiko Yoshida is with the Power Distribution System Plant and Transmission & Distribution Systems Center, Mitsubishi Electric Corporation, Kagawa 763-8516, Japan (e-mail: yoshida.keiko@dw.mitsubishielectric.co.jp).

Takashi Hoshino is with the Transmission & Distribution Systems Center, Mitsubishi Electric Corporation, Hyogo 678-0256, Japan (e-mail: hoshino.takashi@cj.mitsubishielectric.co.jp).

Seiichi Murase is with the Retired in March 2019, (e-mail: smurasehome@ybb.ne.jp).

Hiroshi Murakami is with the MPEC, Hyogo 652–8555, Japan (e-mail: murakami-hiroshi.bv@mpec.co.jp).

Tatsuya Miyashita is with the Mitsubishi Electric Engineering Co., Ltd., Hyogo 661–0001, Japan (e-mail: miyashita.tatsuya@ma.mee.co.jp).

Color versions of one or more figures in this article are available at https://doi.org/10.1109/TPWRD.2020.3025816.

Digital Object Identifier 10.1109/TPWRD.2020.3025816

In [12] and [13], the cores, the winding coils, the insulation oil, and the tank were analyzed using a 3D solid FEM model, so a huge number of model elements would have to be calculated for regular routine works of small core-form transformers..

In [14], to reduce the number of FEM elements, a two-dimensional (2D) finite element model based on axisymmetric elements was used for the coil vibrations. However, the coil model was still overly large for inclusion in a full model that included a tank vibration analysis. The oil was also modeled using a solid mesh, so the tank vibration calculation involved a huge number of elements. The number of numerical elements is very important as an analysis target because the calculations must be light enough to enable design by trial and error of the natural frequency, which must not coincide with the electromagnetic force frequency.

Consequently, we proposed to model the coils using an FEM shell model to enable analysis of the electromagnetic noise characteristics of the small core-form transformer, from which substations are often constructed near residential areas, with minimal simulation times [10]. In the case of the coil model constructed using solid elements, each element size must be smaller than 1/3 of the coil's thickness to express the bending vibration. In contrast, in the case of the coil model constructed using shell elements, in which the elements include the factor for the bending vibration, it is not necessary to divide the elements in the thickness direction, and the mesh size becomes very much larger than that in the solid elements case. The number of model elements when using shell elements becomes less than 1/100 of that of the model using solid elements. In addition, the calculation speed is proportional to the square of the number of elements because the modal analysis matrix calculation size is the square of the number of elements. With regard to our considerations described in Chapters II and III, it is important to avoid having natural frequencies that coincide with the electromagnetic force frequency. Therefore, the natural frequency design must be based on light calculations that designers are able to repeat easily and quickly. We will present an example of the acceleration response calculation required for noise design.

We also proposed vibration propagation analysis of the oil fluid path between the coils and the tank using the boundary element method and vibration analysis of the tank using the FEM [10]. It appears that there are more processes than in the simulation performed using the FEM solid model containing all the elements, which include the coils, the cores, the oil, and a tank. However, the process can be automated and the modeling can be simplified using a size changing tool formatted in Microsoft Excel form that can translate the model to the FEM model, so the engineers have less work to perform for redesigns and can obtain the required answers quickly with light calculation loads. If all elements, including the coils, cores, oil, and tank, are made into the FEM solid model and the vibration and vibration transmission processes of each element are solved using a single FEM process, it is then very difficult to determine the main reason for the acoustic noise and thus find the point at which to remodel. Additionally, if the designers do find the point at which to remodel, they must then repeat the simulation with a model with a huge number of elements. Therefore, we recommend a simulation process that is divided into solving for the vibration responses of the coils, the vibration transmission path of the oil to the tank, and the noise radiation from the tank; this allows the remodel points to be found quickly and the improvements to be confirmed by the remodels.

We demonstrate our proposed noise analysis process steps and the analytical technique for the load noise for two practical transformers in this paper. We also show the noise propagation to the site boundary line, which is the focus of the environmental impact analysis.

II. Vibration of Coils

A. FEM Shell Modeling for the Coils and Tank

A small core-form transformer mainly consists of cores, winding coils, insulation oil, and a tank. High voltage (HV) coils are formed disks by rolling a wire like a worsted yarn, and piled up while inserting spacers. Low voltage (LV) coils, in contrast, are wound up singly to form cylinders.

These types of structure, in which the coils are shaped as disks or cylinders, often include bending vibration modes. If we describe the mode shapes using solid elements, we must then mesh more than three layers in the thickness direction. In addition, if we include the influence of the fluid acting toward the tank, we must use a small solid mesh for the fluid and the sizes of the structural meshes, e.g., those of the coils, cores, or tank, must be adjusted to the size of the fluid mesh. As a result, a huge number of FEM meshes is required.

To solve this problem, we use shell elements for the coils' bending vibration modes and the tank's vibration modes that affect the fluid mass.

B. Basic Theory of Electromagnetic Forced Vibration Response

First, we obtain the vibration modes of the structure using the shell FEM model of the coils. The acceleration frequency response can be expressed using the well-known expression given in [15]:

$$\{a\,(f)\} = \sum_{r=1}^{N} \frac{1}{m_r} \frac{\{\phi_r\}^T \{F\,(f)\} \{\phi_r\}}{\left(\frac{f_r}{f}\right)^2 - 1 + j\eta_r \left(\frac{f_r}{f}\right)}, \tag{1}$$

where f is the frequency; $a(f)$ is the acceleration frequency response; $\{a(f)\}$is the acceleration frequency response at each point; m_r is the *r*th mode mass; ϕ_r is the *r*th mode shape displacement; f_r is the *r*th mode natural frequency; η_r is the *r*th mode loss factor; $F(f)$ is the force at frequency *f*; $\{F(f)\}$ is the force at frequency *f* at each point; and $\{\}^T$ is the transpose of a matrix.

The electromagnetic force of a coil is calculated using the Lorentz force, which is given by the well-known expression

$$\vec{F} = \overrightarrow{I}\ \vec{B}, \tag{2}$$

where $\vec{F}$ is the electromagnetic force; $\vec{I}$ is the electric current; and $\vec{B}$ is the magnetic flux density.

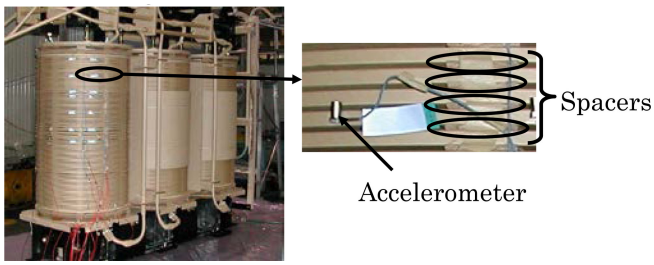

Fig. 1. Accelerometer mounting conditions used for each coil to investigate the amplitude and phase between the coil positions.

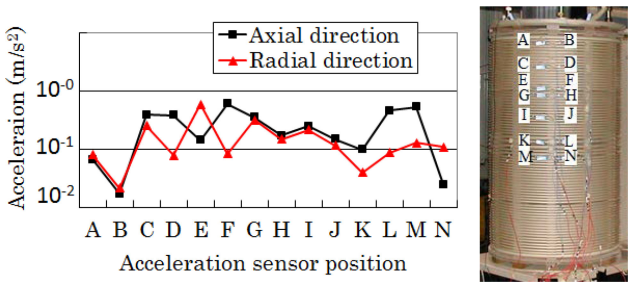

Fig. 2. Comparison of the two vibration directions of the coils. The vertical axis is the amplitude of the acceleration. The horizontal axis represents the sensor positions shown in the photograph on the right.

The electromagnetic force appears in the right angle direction of the magnetic field and the electric current. The HV coil disk is formed using three layers of induction coils. Because $\vec{B}$ in (2) is generated by $\vec{I}$, $\vec{F}$ thus has dimensions given by the square of $\vec{I}$. In addition, the frequency f in (1) must be twice the current frequency, i.e., if the current frequency is 50 Hz, then f in (1) must be 100 Hz.

C. Vibration Response Example of Practical Transformer

We investigated the coil vibration of the transformer through electrical current testing and numerical simulations. A relatively small transformer (66 kV, 3 MVA) was used because the accelerometers had to be attached to the coils directly using double-sided tape and because larger transformers may have suffered some electrical isolation problems when the same installation scheme was used for the accelerometers.

We did not use a 3D laser Doppler vibrometer in this case because we wanted to measure the vertical and horizontal directional accelerations on the curved surfaces of the coils.

The accelerometer mounting conditions for each of the coils are shown in Fig. 1.

As shown on the left side of Fig. 1, the transformer consists of three phase coils. By considering the symmetry of the mechanical form, we measured the accelerations of the top half of one phase coil. The right-hand side of the figure shows the setting used to perform the axial direction acceleration measurements. The radial direction accelerations were measured by varying the directions of the accelerometers.

A comparison of the two directional vibrations is provided in Fig. 2. We have found that accelerations in the radial direction

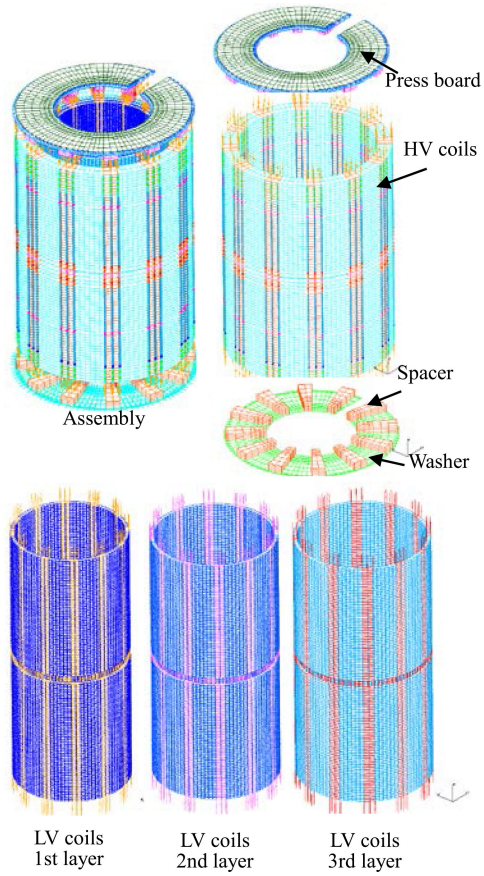

Fig. 3. Numerical models of the transformer coils used for the finite element analysis simulations.

cannot be ignored. The simple mass points -spring analysis, in which the coils are modeled as mass points and the spacers used for electrical isolation between the coils are modeled as springs in the axial direction only, is not able to detect the radial vibrations.

Fig. 3 shows the numerical 3D simulation model of the transformer shown in Fig. 1. We modeled the coil disks and the cylinders using shell elements. Only the high voltage (HV) coils are visible in Fig. 1, but low voltage (LV) coils are also located inside these HV coils. It is difficult to measure the acceleration of the LV coils, so we used the experimental acceleration results for the HV coils shown in Fig. 1 for comparison with the simulation results. The LV coils are shaped like cylinders and each contains a single roll of 99 stacked copper wires wrapped by insulation paper, which total thickness is 9.1 mm. The outer diameters of the first, second, and third layers of the LV coils are 356.8 mm, 389.4 mm, and 399.2 mm, respectively. The HV coils are shaped like 74 stacked disks containing triple rolls of copper wires wrapped by insulation paper, which total thickness is 8.6 mm. The outer diameter of the HV coils is 584 mm. The LV and HV wires have a Young's modulus of 117 GPa, a Poisson ratio of 0.34, and density of 8900 kg/m^3. 12 spacers, which are 40 mm wide and 106 mm long, are inserted between each HV coil disk pair for insulation. The spacer thickness T varies within the 3.5 mm $\leq T \leq$ 12.6 mm range, depending on the cooling or wiring setup. The

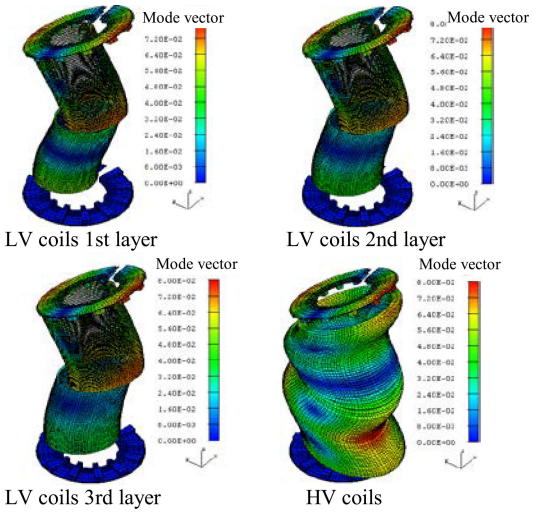

Fig. 4. Mode shapes at the natural frequency of 97.1 Hz of the coils of the transformer obtained by finite element analysis simulations.

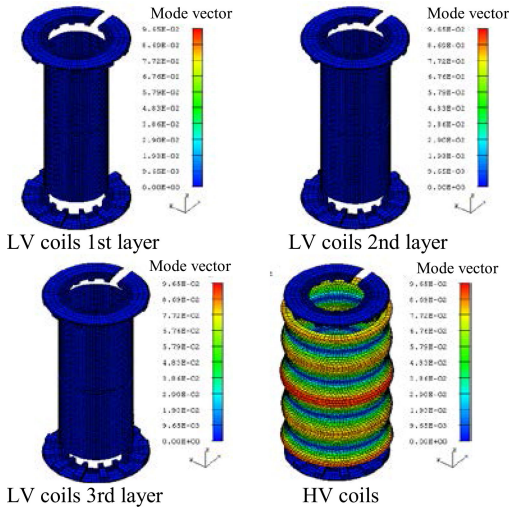

Fig. 5. Mode shapes at the natural frequency of 99.3 Hz of the coils of the transformer obtained by finite element analysis simulations.

spacers between the HV coils were modeled to have the effects of springs in both the axial and radial directions. The spring constant of each spacer among the HV coils was calculated using the spacer's Young modulus of 11 kgf/mm^2 [10] multiplied by the area and divided by the thickness. Our models using the shell elements were verified using the experimental mode analysis presented in our earlier paper [10].

The electromagnetic force frequency is twice the value of the rated frequency. In the case of this transformer, the rated frequency was 50 Hz, so the response must be simulated at 100 Hz. We should note here that the calculation results for the natural frequencies of such high-order modes (more than 30 modes within 100 Hz) usually include an error rate of more than 10%. In this case, the noise levels of the 80 Hz–120 Hz frequency range are calculated.

All vibration modes below 200 Hz must be considered in (1) to examine the effects of the higher mode residual flexibilities [16].

Examples of the vibration mode simulation results obtained from this model using the FEM software NASTRAN are shown in Figs. 4 and 5. We selected representative results near the electromagnetic force frequency of 100 Hz. The vibration modes of all the coils shaped the bending vibration modes of the cylinders.

The electromagnetic forces for each layer of the HV coils that were calculated using the electromagnetic field analysis are shown in Fig. 6. We selected the tap position where the current was lowest because the electrical noise effect there was the lowest during the acceleration measurements, so some coils had no current flow. By considering the vibration with respect to the whole structure as being influenced by the LV coils, as in Fig. 3, we included the LV coils in the acceleration response calculated using (1) and calculated the electromagnetic forces of the LV coils as shown in Fig. 7. In Figs. 6 and 7, the horizontal axis is the coil number, where a lower number represents a higher position in Fig. 3. The vertical axis represents the force, where a negative value means that the phase of vibration of the coil is opposite

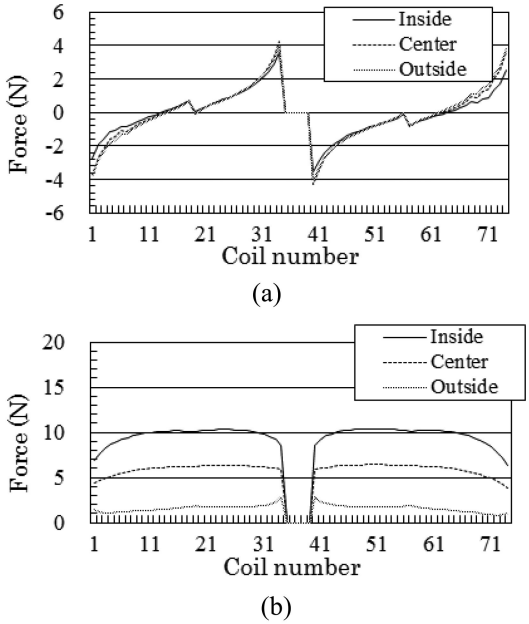

Fig. 6. Electromagnetic force for each layer of the HV induction coils. The coils are numbered in order from the low positions. (a) Axial direction. (b) Radial direction.

to that of another coil. For example, in the axial direction forces of the HV coils, the force between the upper coils with numbers higher than no. 36 and the lower coils with numbers lower than no. 39 have an opposite-phase relationship. In the radial direction forces of the HV coils, the force between the upper coils with numbers higher than no. 35 and the lower coils with numbers lower than no. 40 have the same phase relationship.

The vibration response is obtained by substituting the electromagnetic forces from Figs. 6 and 7 for $F(f)$ in (1) and the loss factor for each of the modes, defined as 0.01, is shown in Fig. 8. In Fig. 8, the experimental data in each direction are the same as those shown in Fig. 2. The vertical axis represents the acceleration level. The conventional model calculation data

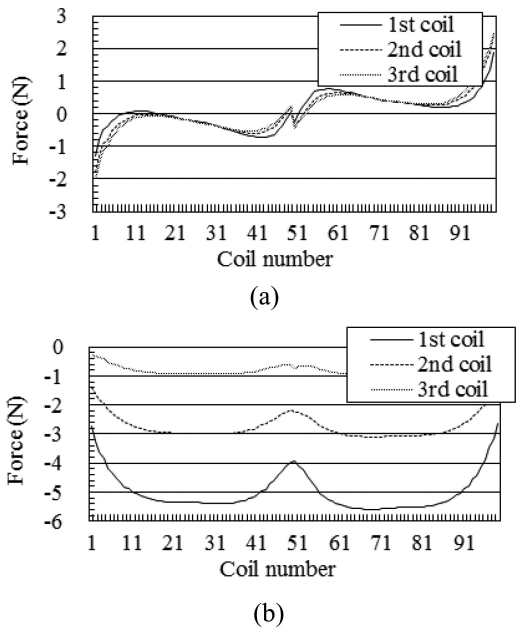

Fig. 7. Electromagnetic force for each layer of the LV induction coils. The coils are numbered in order from the low positions. (a) Axial direction. (b) Radial direction.

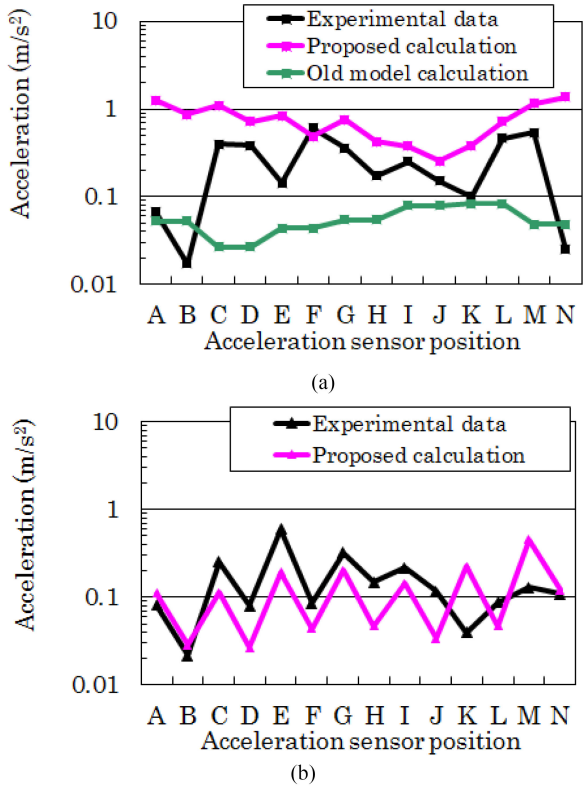

Fig. 8. Comparison of HV induction coil vibration responses between the experimental data and calculated data. (a) Axial direction. (b) Radial direction.

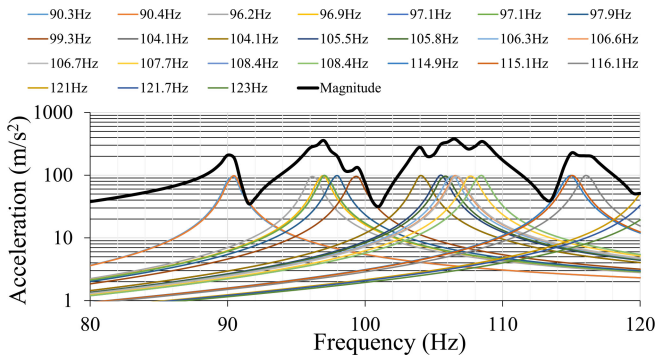

Fig. 9. Acceleration response indicator results calculated using (3).

shown in Fig. 8(a) were calculated using the model in which the coils are modeled as mass points and the spacers used for electrical isolation between the coils are modeled as springs in the axial direction only. There are no data from this model shown in Fig. 8(b) because the model cannot consider the radial directional force. In Fig. 8(a), the proposed calculation data are closer to the experimental data than those obtained from the conventional model, and the accuracy of our proposed calculation model is higher than that of the previous model in the axial direction. However, the accuracies at points A, B, and N became worse than the corresponding values at the other points. The simulation models used were only the coils shown in Fig. 3, which do not consider the top pressboard boundary condition. In fact, the coils, including the pressboard, were set on the cores, so the vibration was suppressed by the core.

In the frequency range of interest, the vibration modes are high enough for the bending wavelength of the coils to be shorter than the coil height. Therefore, the acceleration at the other points can be used to express the vibration levels and shapes.

The calculated data tend to be the same as the experimental data in the radial direction, as shown in Fig. 8(b). This demonstrates that the proposed model can express the coil model vibrations more accurately than the previous method. There are 24 vibration modes in the range between 80 Hz and 120 Hz and each of these vibration modes have an effect on the 100 Hz vibration response. The vibration mode calculation error has a significant effect on the vibration amplitude calculation error, as shown in (1).

For consideration of this error, the acceleration response indicator, $a_{\mathrm{ind}}(f)$, is calculated using the acceleration frequency response calculation results from (1) when assuming a one input–one output system, and the electromagnetic force, where the mode mass is 1, which is defined as in (2).

$$a_{\mathrm{ind}}(f) = \sum_{r=1}^{N} \frac{1}{1} \frac{\begin{Bmatrix} 1 \\ 0 \\ 0 \\ \vdots \end{Bmatrix} \{1, 0, 0, \cdots\} 1}{\left(\frac{f_r}{f}\right)^2 - 1 + j\eta_r \left(\frac{f_r}{f}\right)}, \tag{3}$$

In this case, $a_{\mathrm{ind}}(f)$ is as shown in Fig. 9. In Fig. 9, the bold black line represents the amplitude of the calculation response obtained using (3), and the other lines are the components of each of the natural frequencies f_r from the summation of (3). The black bold line also represents the acceleration results in the case where the natural frequencies are calculated with errors

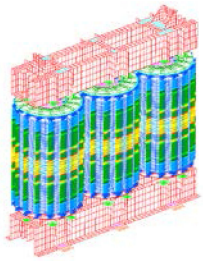

Fig. 10. Numerical model of the coils and cores for the finite element analysis simulation.

with respect to the true natural frequencies. For example, if all the calculated natural frequencies agree with the actual natural frequencies, the acceleration response becomes 75.3 m/s^2 at 100 Hz. However, if all the calculated natural frequencies have a 3 Hz error with respect to the values of the actual natural frequencies, the acceleration response becomes 357 m/s^2, because there are five natural frequencies (96.2 Hz, 96.9 Hz, 97.07 Hz, 97.09 Hz, and 97.9 Hz) that are concentrated near the electromagnetic force frequency. The difference between the maximum and minimum values of the black bold line represents the possibility of an acceleration simulation error being caused by the natural frequency calculation error. Fig. 9 also shows the risk of matching of the natural frequency with the electromagnetic force frequency.

If a transformer is calculated for which some frequencies are concentrated near the electromagnetic force frequency, we can then adjust these natural frequencies to be apart from the electromagnetic force frequency by changing the area of the spacers between the HV coils or the diameters of the LV coils. The spring constant of each spacer between the HV coils is proportional to the spacer area. The mode shapes at each natural frequency, like those shown in Fig. 4 or Fig. 5, are also helpful in finding the structure that must be changed.

We designed this transformer to prevent the natural frequencies from occurring near the electromagnetic frequency of 100 Hz. As a result of this design, the noise level of this transformer was so low that it could not be heard over the 40 dB background noise of the factory.

D. Vibration Response Simulation of Second Practical Transformer (Relatively Larger Device)

Fig. 10 shows the numerical 3D simulation model of a second transformer that is larger than that in Section C. This model involves 4 LV coils shaped as cylinders and 1 HV coil shaped as a disk, like those shown in Fig. 3. This model involves the core structure for consideration of the top pressboard boundary condition.

The LV coils are cylindrical and each coil contains a single roll of 99 stacked copper wires wrapped by insulation paper, which total thickness is 13.5 mm. The outer diameters of the first, second, third, and fourth layers of each LV coil are 499 mm, 537 mm, 575 mm, and 613 mm, respectively. The HV coils are shaped like 84 stacked disks containing four rolls of copper wires wrapped by insulation paper, which total thickness

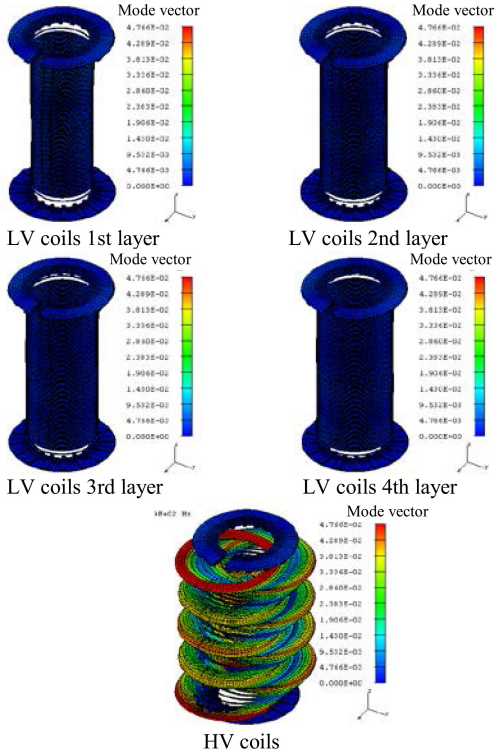

Fig. 11. Mode shapes at the natural frequency of 119.9 Hz of the coils of the transformer produced by finite element analysis simulation.

is 11.4-mm. The outer diameter of the HV coils is 830 mm. The moduli of the wire and spacer materials are the same as those of the previous transformer. 16 spacers, which are 40 mm wide and 150 mm long, are inserted between each HV coil disk pair for insulation. The thickness T of the spacers varies within the 2.9 mm $\leq T \leq$ 12.3 mm range, depending on the cooling or wiring.

In the case where the rated frequency of this transformer is 60 Hz, the response must be simulated at 120 Hz. We should note here that the calculation results for the natural frequencies of such higher order modes (more than 100 modes within 120 Hz) usually include an error rate of more than 10%. In this case, noise levels of 100 Hz–140 Hz were calculated.

Examples of the vibration mode simulation results obtained for this model using NASTRAN FEM software are shown in Figs. 11 and 12. We selected representative results near the electromagnetic force frequency of 120 Hz. There are 203 modes of the LV and HV coil vibrations in the range up to 140 Hz, where the mode at 119.9 Hz is the 106th mode and the mode at 120.0 Hz is the 107th mode. The vibration modes of all the coils are shaped like the bending vibration modes of cylinders. The number of bellies in the vibration modes is higher than those in Fig. 4 and Fig. 5. A larger transformer has more vibration modes than a smaller transformer within the same frequency range.

In a similar manner to Fig. 9, the results for the acceleration indicator $a_{\mathrm{ind}}(f)$ calculated for this case using (3) are shown in Fig. 13. In Fig. 13, the acceleration levels are likely to remain at higher levels than those in Fig. 9 because of the number of natural frequencies that exist close together within the narrow frequency band. A small transformer like that in Section C is easy to

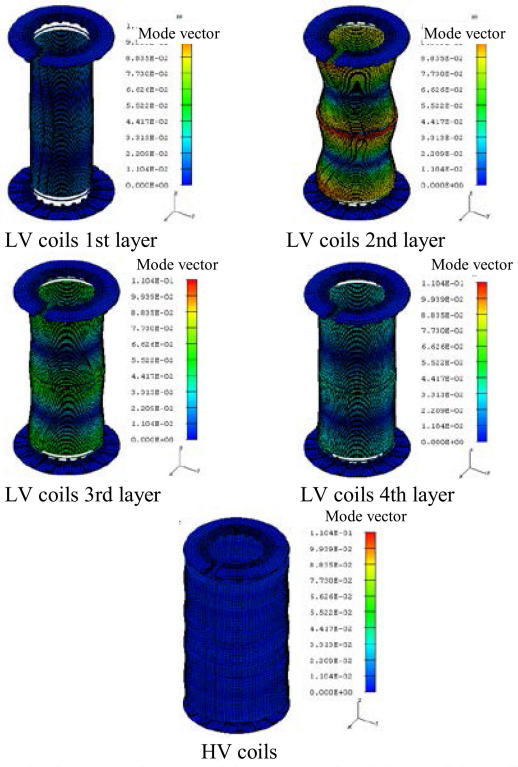

Fig. 12. Mode shapes at the natural frequency of 120.0 Hz of the coils of the transformer produced by finite element analysis simulation.

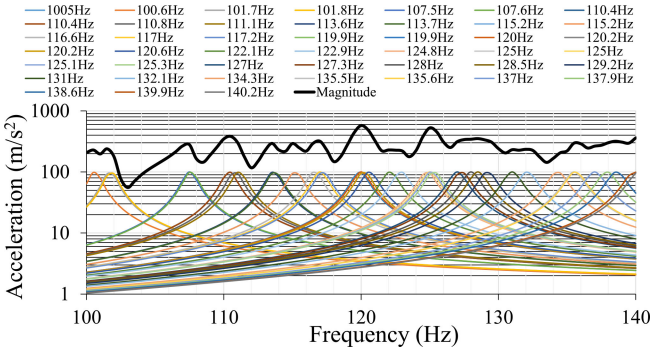

Fig. 13. Acceleration response indicator results calculated using (3).

design with a natural frequency that avoids the electromagnetic force frequency but in this case, it is not easy to design the transformer with a natural frequency that avoids coinciding with the electromagnetic force frequency because there are too many natural frequencies within the operating frequency band. However, if the natural frequency calculation error is less than ± 20 Hz, the largest error is less than 20 dB because the highest level is 575.3 m/s^2 and the lowest level is 55.5 m/s^2, as shown in Fig. 13. This vibration level error influences the noise level error, which will be described in Chapter VI. Additionally, in the higher frequency band, there are so many natural frequencies, i.e., the mode density becomes high, that the probability of an acceleration response becomes rather higher than that in the lower frequency band. It is important to construct the structures of the coils, including the spacers, by increasing their rigidity.

III. Noise Analysis of Transformer Coils

Next, we analyzed the noise around the transformer using the coil vibrations obtained using our proposed shell model-based FEM analysis technique, which was discussed in the previous section. Before performing the noise analysis, we must first obtain the vibration of the tank, which becomes the noise source for the sound receiving points located around the tank as part of the standard test at the factory or on the site's boundary line. There are two vibration propagation paths from the coil to the tank, i.e., the oil and the mounting components between the transformer and the tank.

Here, we use the transformer that was used in Chapter III, Section D, which has a signal-to-noise ratio, i.e., the transformer noise versus the background noise of the factory, that is higher than that of the other transformer.

A. Basic Theory of Transmission Through Fluid by Boundary Element Method (BEM)

We used the BEM to analyze the transmission from the coil vibrations to the tank through the oil and from the tank vibrations to the sound receiving points located around the tank as part of the standard test at the factory. Rather than the BEM, the ray tracing method (RTM) is used to analyze the transmission to the sound receiving points on the site boundary line from the vibrations of the tank or the sound insulation wall bodies surrounding the tank. Because a substation includes multiple obstacle constructions over the distance from the noise source to the site boundary line, we can obtain the results more quickly using the RTM than when using the BEM [17], [18]. The RTM is a classical analytical method and is described in more detail in Section D.

The BEM is a numerical computational method for solution of linear partial differential equations that have been formulated as integral equations. This method attempts to use the given boundary vibrational conditions to fit the acoustic boundary values into an integral equation. Using the Green's function ϕ, which satisfies the scalar wave equation, the sound pressure at point q on a boundary area S is defined as [19]:

$$p_q = -\frac{1}{2\pi} \iint_S \left\{ \phi \frac{\partial p}{\partial n} - p \frac{\partial \phi}{\partial n} \right\} dS, \tag{4}$$

where p_q is the sound pressure at point q; $\frac{\partial p}{\partial n}$ is the partial differential function of the sound pressure in the normal direction; S is the boundary area; ϕ is the Green's function, defined as $\frac{e^{-jkr}}{r}$; r is the distance between point q and each point of S; k is the wave number (ω/c); ω is the angular frequency; and c is the speed of sound.

For the numerical simulations, (4) can be derived by discretizing the boundary area S into N elements, as

$$p_l = -\frac{1}{2\pi} \sum_{m=1}^{N} \frac{\partial p_m}{\partial n} \iint_{S_m} \phi_{lm} dS - p_m \iint_{S_m} \frac{\partial \phi_{lm}}{\partial n} dS, \tag{5}$$

where p_l is the sound pressure at element l; $\frac{\partial p_m}{\partial n}$ is the partial differential function of the sound pressure at element l in the normal direction; r is the distance between elements; ϕ_{lm} is the

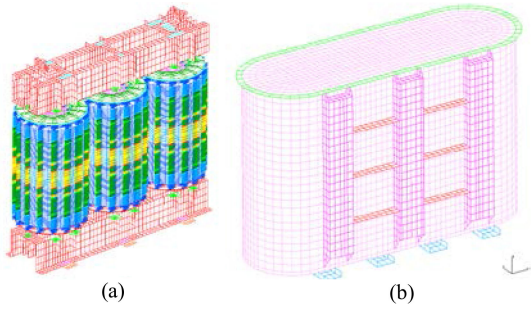

Fig. 14. Coils, cores, and tank model of the transformer used for the acoustic BEM numerical calculations. (a) Coils and cores. (b) Tank.

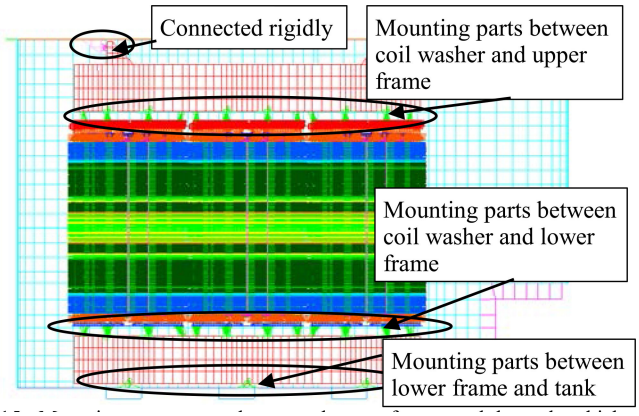

Fig. 15. Mounting components between the transformer and the tank, which is one of the vibration transmission paths from the coil to the tank.

Green's function of distance between element *l* and element *m*; S_m is the area of element *m*; and $\frac{\partial \phi_{lm}}{\partial n}$ is the partial differential function of the Green's function between element *l* and element *m* in the normal direction.

$\frac{\partial p_m}{\partial n}$ is derived as an acceleration using (1), which multiplies the partial mass of element *m* as follows:

$$\frac{\partial p_m}{\partial n} = -\rho a(f) \tag{6}$$

To calculate (5), we used the LMS International SYSNOISE software that is integrated into the Siemens Simcenter software system [20].

B. Numerical Model and Simulation Procedures for Acoustic Noise Response Around Transformer

In this section, we focus on the acoustic noise response around the transformer in the factory test performed before shipping. The numerical model of the coils and the tank is shown in Fig. 14. The models of the coils and cores from the vibration simulation model of Fig. 10 were applied and the vibration acceleration results are substituted for $a(f)$ in (6). The width, length, and height of the tank are 3418 mm, 1300 mm, and 2409 mm, respectively. The tank thickness is 9 mm and some parts have reinforcement members with thickness *T* that varies within the 9 mm $\leq T \leq$ 12 mm range. The vibration acceleration of each phase coil is given a phase difference of 120 degrees with respect to each other. The coil washer is placed on the base of the transformer and fixed at 6 degrees with respect to the tank. The tank is made from steel (SS400) and is filled with oil with a density of 900 g/m^3. The tank is constructed from steel panels with vibration modes that are influenced by the oil fluid mass [14] [21], so the modal analysis of the tank is performed using a fluid–structure coupled analysis. We used NASTRAN MFLUID analysis [21] to perform the fluid–structure coupled analysis.

The simulation procedures for noise transmission via the oil i.e., structure-fluid coupled sound, are described as follows.

1) The acceleration $a(f)$ of the coils in (1) is calculated by substituting for the electromagnetic force $F(f)$ calculated using $\vec{F}$ in (2).
2) The sound pressure of the oil at the tank wall boundary is calculated using (6) based on the acceleration $a(f)$ of the coils.
3) The vibration modes, i.e., m_r, ϕ_r, and f_r in (1), for the tank with oil are analyzed via the fluid–structure coupled analysis.
4) The acceleration $a(f)$ of the tank wall in (1) is calculated by substituting for the acoustic pressure of the oil at the boundary of the tank wall $\times$ the numerical mesh element area calculated using $\vec{F}$ in (2).
5) The sound pressure at the boundary of the sound receiving point mesh, which is arranged around the tank at the factory, is calculated using (6) with the acceleration $a(f)$ of the tank wall.

Additionally, the coil vibration propagates to the frame through the mounting components, and the frame vibration then propagates to the tank. The simulation procedures for noise via the connecting structure (mounting components), i.e., structure-borne sound, are described as follows.

1) The vibration modes, i.e., m_r, ϕ_r, f_r in (1), of the whole model, including the coils, the frames, and the tank with oil, are analyzed via the fluid–structure coupled analysis.
2) The acceleration $a(f)$ in (1) for the tank wall is calculated by substituting for the electromagnetic force $F(f)$ in (1).
3) The sound pressure at the boundary of the sound receiving point mesh is calculated using (6) along with the acceleration $a(f)$ of the tank wall.

The numerical model of the interior of the tank and the mounting components between the transformer and the tank (which is one of the vibration transmission paths from the coil to the tank) is shown in Fig. 15. The steel core is connected to both the upper and lower frames. The vibration of the steel core is not considered in this case; only the mass and connection effects for the frame are considered.

The actual noise simulation is led by the summation of the noise caused by the tank vibration propagating from the coils via the oil.

C. Simulation Results for the Noise Level in the Factory

Examples of the contour maps of the calculated results for the sound pressure level (SPL) and the noise level (A-weighted SPL) at the sound receiving points (called 'the field point mesh'

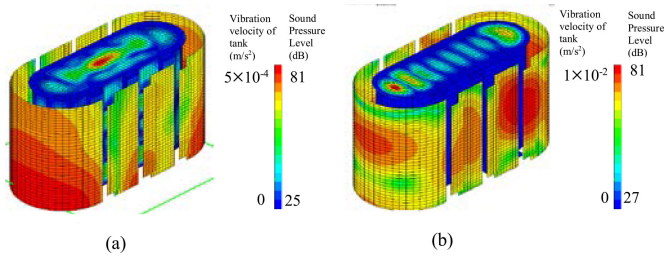

Fig. 16. Calculation results of the sound pressure level (SPL) contour map and the maximum noise level (A-weighted SPL) at 120 Hz. (a) Structure-fluid coupled sound at 120 Hz Max noise level: 75 dB). (b) Structure borne sound at 120 Hz (Max noise level: 64 dB).

TABLE I
MAXIMUM NOISE LEVEL CALCULATION RESULTS

Frequency	Structure-fluid coupled sound	Structure borne sound
100 Hz	54dBA	47dBA
110 Hz	61dBA	54dBA
120 Hz	75dBA	64dBA
130 Hz	54dBA	47dBA
140 Hz	61dBA	66dBA

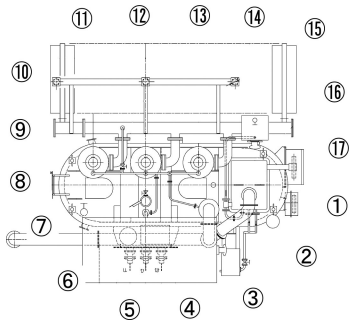

Fig. 17. Noise level measuring points from top view for the transformer noise level definition.

in SYSNOISE) at 120 Hz are shown in Fig. 16. The contour maps of the vibration levels of the tank are also shown. The maximum noise level at each frequency is shown in Table I.

The transformer noise level measurement points are shown in Fig. 17. These points were measured at a distance of 30 cm away from the tank wall. The heights of these measurement points are at 1/3 and 2/3 of the transformer height. As such, the sound receiving point mesh for procedure 3 is constructed on an exterior plane located 30 cm away from the tank wall.

The noise level calculation points on the sound receiving points of the simulations are shown in Fig. 18. These calculation points are located at almost the same positions as the measurement points.

The measurement results for the noise levels at each point in Fig. 18 are shown in Table II and a comparison between the measurement results and the calculated results is shown in Fig. 19. In Fig. 19, the measurement results exist within the range of the calculation results from 100 Hz–140 Hz. To be on the safe side, and because of the number of modes present, we recommend in the actual noise design that the electromagnetic noise be calculated within a frequency range of ±10% of twice the rated

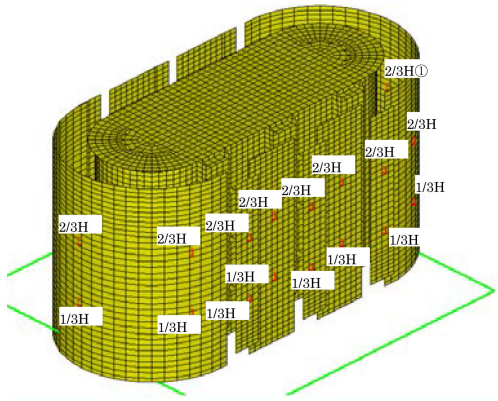

Fig. 18. Noise level calculation points for the transformer noise level for comparison with the measurement results.

TABLE II
NOISE LEVEL MEASUREMENT RESULTS (BACKGROUND NOISE: 43.8 dBA)

Point number	Noise level dBA		Point number	Noise level dBA	
	1/3 height	2/3 height		1/3 height	2/3 height
1	48.0	51.0	11	53.5	50.5
2	53.0	50.5	12	48.0	45.5
3	47.0	48.5	13	48.0	49.0
4	49.0	45.5	14	45.5	50.0
5	46.5	48.0	15	47.0	46.5
6	48.0	49.5	16	46.0	46.0
7	52.0	51.5	17	54.5	49.0
8	48.0	48.5			
9	49.0	48.0	Average	49.3	
10	44.0	48.5	background noise correction	48.3	

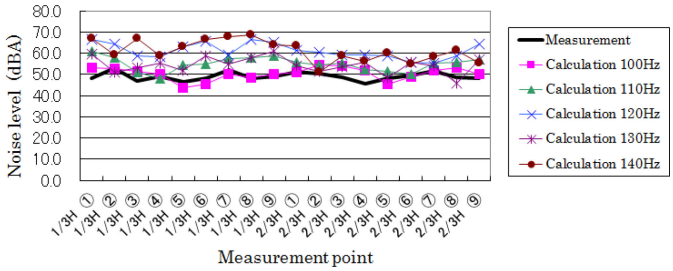

Fig. 19. Comparison of noise levels between measurements and calculations. The horizontal axis represents the height ratio of the transformer.

frequency of the transformer. In Fig. 19, the dispersion range of the noise levels of the calculated results is approximately 20 dB. This range is nearly equal to that of the acceleration response shown in Fig. 13. If there are few natural frequencies near the electromagnetic force frequency, such as those of the transformer considered in Fig. 9 in Chapter II, Section C, we can set the natural frequencies to be apart from the electromagnetic force frequency through structural design. However, when there are many natural frequencies near the electromagnetic force frequency, it becomes more difficult to set these natural frequencies apart from the electromagnetic force frequency. We must design the transformer by assuming the worst case scenario and thus

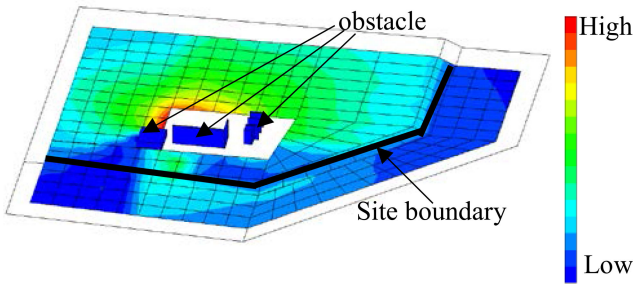

Fig. 20. Example noise calculation results for site boundary. Counters are noise levels on the premises and the noise propagation characteristics.

recommend performing the simulation within a frequency range of ±10% and also make the structures of the coils, including the spacers, as rigid as possible. In the case of the transformer considered here, the natural vibration frequencies in this range are considered to have been calculated as being lower than that of the practical transformer. In other words, the structures of the coils and spacers of this transformer are constructed with higher rigidity than in the assumption made in the simulation. As a result, the measurement data became close to the lowest noise simulation results attained at 100 Hz.

D. Noise Propagation for Site Boundary Line

The noise level on the site boundary line must be lower than the environmental low level for each region. If the substation is located near a residential area, some special treatment is required for the environmental noise.

Usually, when the outdoor noise level measurement point is located more than several meters away from the noise source, it is analyzed using the ray tracing method (RTM), which is a conventional computational calculation method [17], [18], [22], [23] that is often used in architectural acoustics in particular and considers the diffractions and reflections of acoustic waves.

The level of noise at the site boundary line that is caused by the transformer is calculated using RAYNOISE [23]. This software is integrated into the Siemens Simcenter software system [24]. An example of the noise calculation results at the site boundary line is shown in Fig. 20.

If the transformer is covered using some sound insulation walls, the noise source for the site boundary line is then considered to be the sound insulation wall. The vibration of the sound insulation wall can be calculated in the same way that we calculated the vibration of the tank (see parts A and B). The space between the tank and the wall is filled with air, so the fluid in the calculation in step 3 of the fluid–structure coupled analysis is air and can be applied to perform an air–structure coupled analysis. The analytical scheme for the transformer specifications and the geographical features of the substation, including the sound insulation walls, are shown in Fig. 21.

IV. Conclusion

For electromagnetic noise analysis of a transformer, we proposed the use of a shell element-based FEM model for the numerical model that enabled lighter computational simulations, and

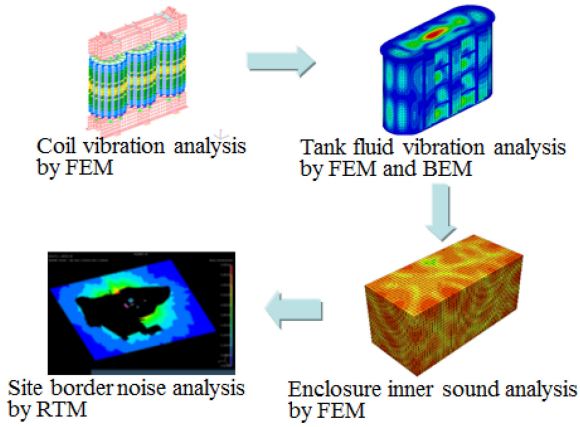

Fig. 21. Diagnostic routine for transformer noise.

division of the simulation process into each structural vibration, transmission path, and radiation process makes it easier to find the remodel point than performing the complete simulation at one time. We presented a calculation example that involved designing the natural frequency to be apart from the electromagnetic force frequency. These noise reduction considerations need to be calculated quickly during the design process.

Acknowledgment

The authors thank David MacDonald, MSc, from Edanz Group for editing a draft of this manuscript.

References

[1] M. J. Heathcote, *The J&P Transformer Book*, 12th edition. Oxford, U.K.: Newnes, 1998.
[2] A. Kudo, T. Nishitani, T. Yoshikawa, and C. T. Wanm, "Development of 275kV gass cooled tupe gas-insulated power tranformer," *IEEE Trans. Power Del.*, vol. 8, no. 1, pp. 264–270, 1993.
[3] A. W. Kelly, "Measurement of spacecraft power transformer acoustic noise," *IEEE Trans. Magn.*, vol. 26, no. 1, pp. 281–289, 1990.
[4] B. Weiser, H. Pfutzner, and J. Anger, "Relevance of magnetstriction and forces for the generation of audible noise of transformer cores," *IEEE Trans. Magn.*, vol. 36, no. 5, pp. 3.759–3777, 2000.
[5] A. J. Moses, "Measurement of magnestoriction and vibration with regard to transformer noise," *IEEE Trans. Magn.*, vol. 10, no. 2, pp. 154–156, 1974.
[6] JFE Steel Corporation Catalog, "Super Core TM, electrical steel sheets for high-frequency application," Japan. [Online]. Available: http://www.jfe-steel.co.jp/en/products/electrical/catalog/f1e-002.pdf, Accessed on: Jul. 27, 2020.
[7] S. Takajo, T. Ito, S. Okabe, and T. Omura, "Loss and noise analysis of transformer comprising grooved grain-oriented silicon steel," *IEEE Trans. Magn.*, vol. 53, no. 9, Sep. 2017.
[8] A. Ilo, "Behavior of transformer cores with multistep-lap joints," *IEEE Power Eng. Rev.*, vol. 22, no. 3, pp. 43–47, Mar. 2002.
[9] S. Itoh, H. Murakami, and N. Tsujiuchi, "Transient vibration response of transformer coils under external short circuit," *Trans. Japan Soc. Mech. Engineers Ser. C*, vol. 60, no. 570, pp. 394–398, 1994.
[10] K. Yoshida, T. Hoshino, S. Murase, H. Murakami, and T. Miyashita, "Electro-magnetic noise design of a transformer," *Trans. Japan Soc. Mech. Engineers Ser. C*, vol. 78, no. 789, pp. 1519–1530, 2012.
[11] P. Shao, L. Luo, Y. Li, and Christian Rehtanz, "Electromagnetic vibration analysis of the winding of a new HVDC converter transformer," *IEEE Trans. Power Del.*, vol. 27, no. 1, pp. 123–130, 2012.
[12] H. Jingzhu, L. Dichen, L. Qingfen, Y. Yang, and S. Liang, "Electromagnetic vibration noise analysis of transformer windings and core," *IET Elect. Power Appl.*, vol. 10, no. 4, pp. 251–257, 2016.

[13] F. Yang, Z. Ren, D. Zhang, L. Li, X. Fan, and Y. Zhou, "Simulation analysis and experiment validation of vibration and noise of oil-immersed transformer," in *Proc. 22nd Int. Conf. Elect. Mach. Syst.*, 2019.
[14] M. Rausch *et al.*, "Combination of finite and boundary element methods in investigation and prediction of load-controlled noise of power transformer," *J Sound Vib.*, vol. 250, no. 2, pp. 323–338, Feb. 2002.
[15] R. J. Allemang, "Investigation of some multiple input/output frequency response function experimental modal analysis techniques," Ph.D. dissertation, Univ. Cincinnati, 1980.
[16] A. S. Taylor and M. R. Cllyer, "An assessment of the importance of the residual flexibility of neglected modes in the dynamical analysis of deformable aircraft," Royal Aeronaut. Soc., RAE Tech. Rep. 73119, ARC 35085, 1973.
[17] X. Cai, L. Wang, S. Wang, N. Yao, and D. Li, "Radiation noise prediction of outdoor substation based on improved ray tracing method," in *Proc. INTER-NOISE NOISE-CON Congr. Conf.*, 2017, pp. 3700–3706.
[18] E. A. Piana and N. B. Roozen, "The control of low-frequency audible noise from electrical substations: A case study," *Appl. Sci.*, vol. 10, no. 2, p. 637, 2020. [Online]. Available: https://www.mdpi.com/2076-3417/10/2/637/htm
[19] C. A. Brebbia, *The Boundary Element Methods for Engineers*, Pentech Press, 1975, Transl.: Japanese, BAIFUKAN, 1983.
[20] Simens, Simcenter 3D. [Online]. Available: https://www.plm.automation.siemens.com/global/en/products/simcenter/simcenter-3d.html, Accessed on: Sep. 29, 2020
[21] C. M. Fernholz and J. H. Robinson, "Fully coupled fluid/structure vibration analysis using MSC/NASTRAN," NASA Tech. Memorandum 110215, pp. 1–90, Jan. 1996.
[22] H. Weinberg, "Application of ray theory to acoustic propagation in horizontally stratified oceans," *J. Acoust. Soc. Am.*, vol. 58, pp. 97–109, 1975.
[23] D. E. White and M.A. Pedersen, "Evaluation of shadow-zone fields by uniform asymptotic and complex rays," *J. Acoust. Soc. Am.*, vol. 69, pp. 1029–1059, 1981.
[24] LMS INTERNATIONAL RAYNOISE revision 3.1 Users Manual. [Online]. Available: http://sunileng.biz/pic/etcdata/rn31.pdf, Accessed on: Jul. 27, 2020.

Keiko Yoshida was born in Kochi, Japan. She received the Ph.D. degree in mechanical engineering from Doshisha University, Kyoto, Japan, in 2005. She has been an Engineer of sound and vibration for electrical manufacturing of equipment, including artificial satellites, elevators, air conditioners, telescopes, railway vehicle devices, car devices, and power transformers. She held the position of Mechanical Department Manager of the R&D Center and Design Systems Center from 2013 to 2018 and is currently the Chief Engineer of the Power Distribution System Plant of the Mitsubishi Electric Corporation. She is also engaged in the study of seismic design at the Research and Development Department of the Transmission and Distribution Systems Center. Her awards and honors include the Fellowship of the Japan Society of Mechanical Engineers (JSME) in 2019, the JSME Space Engineering Division Award in 2005, and the JSME Kansai Branch Award in 2007.

Takashi Hoshino was born in Kanagawa, Japan, in 1965. He received the M.S. degree in electrical engineering from the Musashi Institute of Technology, Tokyo, Japan, in 1990. From 1990 to 2012, he was engaged in the development of core-type transformers for Mitsubishi Electric Corporation, Japan. From 2012 to 2015, he was engaged in transformer production management with the Baoding Baoling Transformer Co., Ltd., China and was engaged in a transformer production management position with Mitsubishi Electric Power Products, Inc., USA from 2015 to 2019. Recently, he returned to the Transmission and Distribution Systems Center of Mitsubishi Electric Corporation.

Seiichi Murase was born in Nagoya, Japan, in 1948. He received the M.S. degree in mechanical engineering from the University of Kumamoto, Kumamoto, Japan, in 1978 and the Ph.D. degree from Kyoto University, Kyoto, Japan, in 1991. From 1978 to 2019, he was engaged in vibration testing and analysis of railway rolling stock and seismic testing and analysis of substation equipment in the Research and Development Department of the Transmission and Distribution and Transportation Systems Centers of Mitsubishi Electric Corporation. He is an expert in the fields of seismic design, seismic analysis and seismic testing. He retired from Mitsubishi Electric Corporation in March 2019. He was a recipient of Japan's Minister of Economy, Trade and Industry Award for Distinguished Service to Electrical Safety, in 2020.

Hiroshi Murakami was born in Nagasaki, Japan, in 1958. He received the B.S. and M.S. degrees in mechanical engineering from the University of Kyushu, Fukuoka, Japan, in 1984. From 1984 to 2017, he was engaged in the design and development of power transformers for Mitsubishi Electric Corporation, Japan. Since 2017, he has been engaged in the operation and maintenance of the social infrastructure with the Mitsubishi Electric Plant Engineering Corporation, Japan.

Tatsuya Miyashita was born in Hyogo, Japan, in 1969. He received the graduate degree from Itami Nishi High School, Itami, Japan, in 1987, and the B.S. degree in mechanical engineering from Setsunan University, Osaka, Japan, in 1991. Since 1991, he has been engaged in mechanical engineering of structures, vibrations, acoustics and impact via computer-aided design for the Mitsubishi Electric Engineering Corporation, Japan.